ANNUAL REPORT TO THE LASER FACILITY COMMITTEE 1992

5 April 1991 to 4 April 1992

SERC CENTRAL LASER FACILITY
RUTHERFORD APPLETON LABORATORY
CHILTON
DIDCOT
OXON
OX11 0QX

Telephone 0235 821900
Telefax 0235 445888

Rutherford Appleton Laboratory Report RAL-92-020

Cover design representing chirped pulse amplification and compression used for generating ultra-bright laser beams.

PLASMA CONDITIONS GENERATED BY INTERACTION OF A HIGH BRIGHTNESS, PRE-PULSE FREE RAMAN AMPLIFIED KrF LASER PULSE WITH SOLID TARGETS

D. RILEY, L.À. GIZZI, F.Y. KHATTAK, S.M. VIANA and O. WILLI

The Blackett Laboratory, Imperial College of Science, Technology and Medicine, Prince Consort Road, London SW7 2BZ

Interest in the production of dense, hot plasmas by irradiation of solids with short pulse high power lasers is motivated by the applications to X-ray laser research where rapid heating at high density is required. Several workers have already published experiments in which spectroscopy is used to diagnose dense plasmas created by irradiation of solid targets with laser pulses of sub-picosecond to a few tens of picoseconds duration [1-5].

We have carried out an experiment in which the interaction of the 12ps Raman amplified SPRITE pulse was interacted with solid targets. The Amplified spontaneous emission (ASE) pre-pulse level was not detectable at the threshold of measurement, implying that it is $<10^{-10}$ of the power and 10^{-8} of the energy in the main pulse. For the irradiances of up to 10^{17} W/cm^2 used, no pre-formed plasma should be present during the pulse interaction. The laser was directed onto planar (25μm thick) aluminium foils by an off axis paraboloid, with f/4 effective focussing of about 4J on target.

The main diagnostic of the plasma conditions was a time resolving X-ray spectrometer which consisted of a Tlap crystal coupled to a streak camera which was fitted with a KBr photocathode and viewed the plasma at an angle of approximately 35 degrees to the normal. The temporal and spectral resolutions achieved were approximately 10ps and 350 respectively. Using this instrument, the aluminium K-shell emission between 6 and 7 Angstroms was recorded on film.

For the streak data, the focal spot was monitored via the X-ray emission with a time integrating pinhole camera which was fitted with four separately filtered pinholes of 10μm diameter and had a x15 magnification. The pinhole used to define irradiance was filtered with 25μm Be + 3μm Al, and had greater than 1/e transmission for photon energies above 2.5keV, and so was mainly sensitive to the bremsstrahlung and radiative recombination X-rays generated during the laser pulse. Approximately 90% of the X-ray emission was contained within the FWHM intensity, which was similar to the nominal focal spot set by focussing onto a wire of known thickness. The X-ray emission in several energy bands was monitored with *p-i-n* diodes and the velocity of the ions in the blow-off plasma was monitored with ion cups.

The absorption of the laser pulse was measured as a function of incident angle and intensity by monitoring the energy on target and measuring the scattered light via an Ulbricht sphere and a calibrated diode on a backscatter collection channel. A detailed description of the data collected on the interaction and absorption of the beam with solid targets will be presented at a later date. In this report we concentrate on the plasma conditions generated with this pre-pulse free high brightness laser at normal incidence and irradiances of a few times 10^{15} Wcm^{-2}.

Figure 1 shows a graph of the reflected light versus irradiance for normal incidence on aluminium foils. In the absorption data, the focal spot was defined by moving the target a fixed distance from the smallest focus as observed on a T.V alignment system which viewed the target through a small hole in the Ulbricht sphere. As can be seen, efficient coupling of the laser energy is achieved for irradiances up to 10^{17} Wcm^{-2}. This is understandable in terms of classical absorption arguments in which the moderate Z of the targets and the short wavelength tend to favour inverse bremsstrahlung.

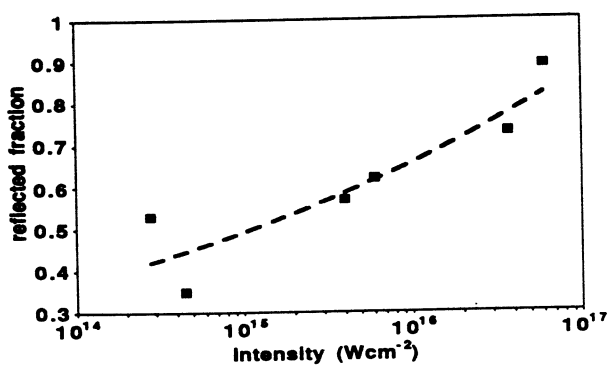

Figure 1. Measured total reflectivity versus incident irradiance for Al foil targets.

Figure 2a shows streak data taken from an aluminium target irradiated at approximately 10^{16} Wcm^{-2}. Note the temporal evolution of the He-like line series from a broad emission band into distinct emission lines, indicating high electron density at the start of the emission. This can be seen clearly in the film density line outs

of figure 2b, which shows a band of emission well above the bremsstrahlung continuum at early time which evolves into distinct Al XII $1s^2$-1s4p (Heγ) and $1s^2$-1s5p (Heδ) transitions. The curvature of the image due to electron path differences in the camera introduces a timing difference across the spectrum of the order of the temporal resolution due to the cathode slit. The width of the AlXII $1s^2$-1s3p (Heβ) line was modelled as described below and indicates an electron density of approximately $1.4x10^{23}$ cm^{-3} for scan(i) in figure 2b. The continuum lowering model of Stewart and Pyatt [7] suggests that for temperatures of a few hundred electronvolts, when He-like emission is strong, the He-like n=5 level is still bound at this electron density. If we assume the plasma to be fully or almost fully ionised, the merging of the Heγ and Heδ lines is consistent with the Inglis-Teller model [8] of line series merging at high electron density.

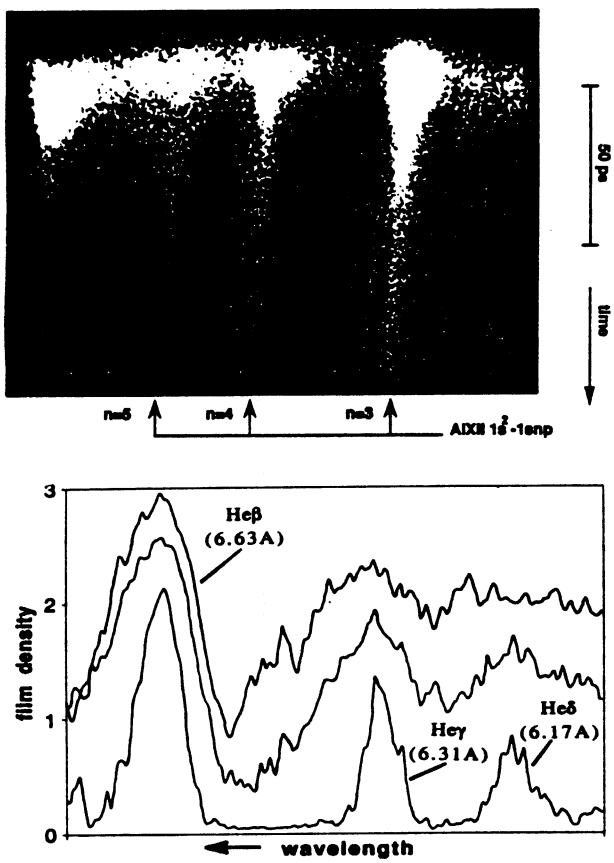

Figure 2. (a) Streaked X-ray spectrum of He-like line series (b) Film density line-outs. Timing is (i) 10ps before peak Lyβ emission, (ii) 10ps later and (iii) 50ps later. Note that scan (i) is displaced in density by 0.3 for ease of viewing.

In order to assess the plasma conditions more closely, we have analysed data on aluminium foils taken with lower dispersion. This means that the AlXIII 1s-3p (Lyβ) transition is included in the spectrum, and the temperature is indicated by the ratio of He-like to H-like emission. The evolution of the Heγ and Heδ lines from a broad band into separate emission lines was also seen for these data shots. The electron density was determined from the Stark width of the Heβ and Lyβ transitions. The variation of linewidth with density for these two lines was calculated using the spectral simulation code SPECTRA [9] which includes detailed Stark profiles for H, He and Li-like lines as well as continuum lowering, opacity, Doppler broadening and instrument width. The temperature was assumed to be 400eV for Heβ and 600eV for Lyβ, but to account for uncertainty in opacity, was varied from 200 to 800 eV and 300 to 900eV for Heβ and Lyβ respectively, with the plasma ρR being varied up to $1.2x10^{-4}$ gcm^{-2}: these conditions span the expected values for the emission region with the foil targets. The variations in predicted density for a given linewidth were then used to set the error bars. A fit of the full line profile was carried out on a few scans; the results obtained were the same as for the FWHM comparison to within the error bars generated. Due to instrument broadening, the linewidth ceased to be sensitive to density below about $3x10^{22}$ cm^{-3}.

The experiment was simulated with a 1-dimensional hydrocode, MEDUSA [10]. The heat flow is given by the smaller of the Spitzer value and a flux limited free streaming limit. From the work of Rickard et al [11], we decided on a flux limit of 0.1. The energy is absorbed by inverse bremsstrahlung and resonance absorption. The amount of resonance absorption is varied with the scalelength [12] at critical density in conjunction with the averaged angle of incidence due to the f/4 focussing. Some of the resonantly absorbed energy is dumped at critical density, with the rest being put into hot electrons which are transported in 10 energy groups with an initial temperature at the critical density surface which is calculated from the expression derived from experiments, by Giovanielli [13]. The fraction of resonantly absorbed energy put into the hot electron population was not found to significantly alter the hydrodynamic behaviour, because the high density and relatively low suprathermal electron temperature, (4.5keV for $I=4.0x10^{15}$ Wcm^{-2}), due to the short laser wavelength meant that the hot electron energy was dumped spatially quite close to the critical density surface anyway. A value of 50% was used for simulations presented here. The ionisation balance is calculated with a time dependent non-LTE average atom, (AA) model similar to XSN [14], which includes reabsorption of the resonance line by use of an escape factor which is determined by the Doppler width. Because the AA model treats ions in a hydrogenic approximation it might be expected to give reasonable results as the plasma is dominated by the He-like to bare ions. A

comparison of the AA model and a detailed ionisation model [7,15] has been made for the steady state case. For electron temperatures between 200 and 900eV and electron density from 10^{22} to 10^{23} cm^{-3} , the two models were found to give the ratio of bare to Hydrogenic ions to within at most a factor of two with differences less than 20% for most of the conditions of interest. The emission intensity of the AlXII $1s^2$-1s3p and AlXIII 1s-3p lines was calculated by assuming that the n=3 levels of H and He-like ions were in local thermodynamic equilibrium (LTE) with the bare and Hydrogenic ground states respectively. Using the usual criterion [16], this should be a reasonable assumption at above critical electron density ($1.6x10^{22}cm^{-3}$). The predicted electron density and temperature was calculated as an emission weighted average over the simulation cells for the H-like and He-like lines separately The effect of hot electrons on the ionisation balance early in time (i.e during the laser pulse) is not included in our ionisation modelling; however, the simulations suggest that few hot electrons will reach the high density plasma from which the early time emission originates and are not expected to significantly alter our conclusions about the plasma conditions.

Figure 3 shows the experimentally inferred electron density compared to predicted averages for an aluminium foil irradiated at $4x10^{15}$ Wcm^{-2}. In order to make the comparison, the time of peak Lyβ emission in the simulation was equated to the experimental peak (timing differences due to image curvature are accounted for). In both simulation and experiment the peaks of the Heβ and Lyβ were separated by less than the experimental temporal resolution. The predicted absorption was 41% which is consistent with the data in figure 1. We can see that the peak electron density and general fall of in density is reasonably well reproduced by the hydrocode but is slightly better for the Lyβ than for for the Heβ line. The agreement of experiment and simulation is better at early time if the escape factors are not used, but is better at late time if they are included. This is possibly due to the invalidity of assuming a Doppler width dominated line profile at early time when the electron density is high. This explanation has to be treated with care as the error bars on the data are larger than the difference in predicted histories.

Figure 4a shows the predicted Heβ/Lyβ line ratio compared to experimental measurement for times when the electron density of the emiting region is above the limit for LTE to apply. The measured ratio generally agrees with the predicted ratio, at the average irradiance, to within a factor of two. In order to

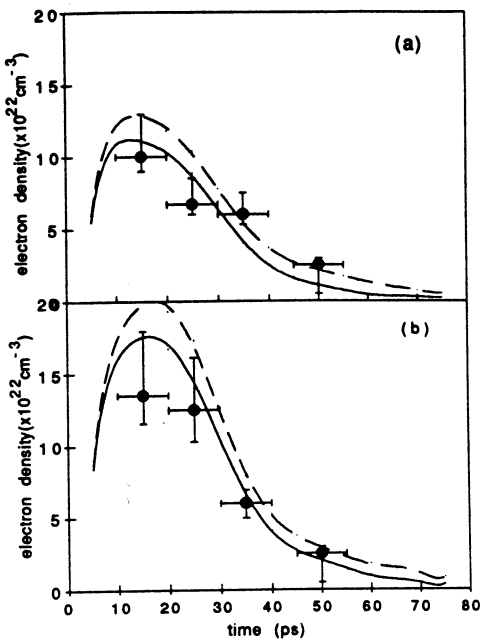

Figure 3. Time history of the electron density inferred by the Lyβ and Heβ linewidths, compared with the simulation, without(——), and with (----) reabsorption of the resonance line. Note that a 10ps window has been folded into the predicted data to simulate temporal resolution.

show the sensitivity to temperature, the simulated ratio is shown for irradiances 50% above and below the average. The predicted typical temperature is taken by finding the emission weighted average temperature in the simulation cells for the He-like and H-like lines separately and taking the mean of these. For the

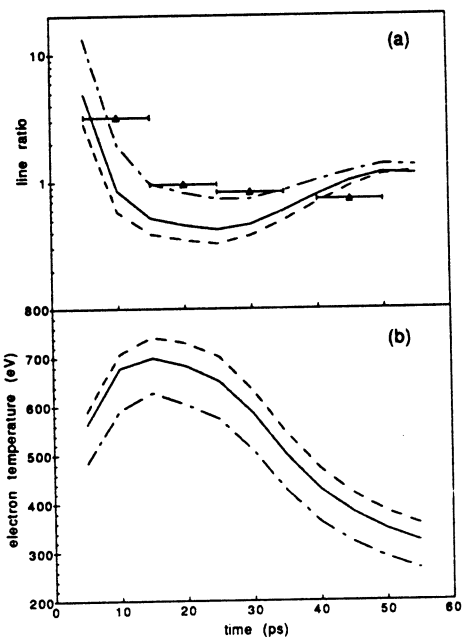

Figure 4. (a) measured Heβ/Lyβ line ratio vs. simulation for irradiances of $6x10^{15}Wcm^{-2}$ (broken line), $4x10^{15}Wcm^{-2}$ (solid line) and $2x10^{15}Wcm^{-2}$ (dot-dashed line). (b) Predicted average plasma emission temperature for the same irradiances, with same line styles as (a). Again a 10ps window is folded into predicted data.

irradiances considered, the predicted temperatures for H-like and He-like emission differ by less than 20% of their average. Figure 4b shows simulated typical plasma temperature for the conditions in figure 4a. As can be seen, the variation in temperature that would bring the predicted and measured line ratios into agreement is generally less than 100eV.

The simulated FWHM duration of emission is 20ps and 25ps for the Heβ and Lyβ lines respectively, which compares well with the value of 25-30ps for both lines from the data. However, the streak data shows a strong tail of emission which lasts for about 100ps. The approximations made in our ionisation model are not appropriate for modelling the coronal plasma late in time, and as the density is below our resolution limit we do not address this phase of the plasma expansion here. This longevity of emission is probably responsible for the fact that time integrated data, taken with this laser [15], indicates electron densities of only a few times 10^{22} cm^{-3}, when it is predicted that most emission will come from substantially higher density. This may also help to explain the smaller linewidths measured by other workers from time-integrated spectroscopy of plasmas created with short pulses.

In order to further reduce the effects of opacity on the linewidth we have also taken data with layered targets. These consisted of a 10μm plastic subtstate onto which was coated a 0.2μm layer of Al and a 0.1μm layer of CH facing the laser. Figure 5 shows spectra taken fomr a layered target irradiated at $6.4x10^{15}$ Wcm^{-2}. Again, we can clearly see the evolution of the He-like series from a broad emission band into distinct transitions. The peak densities for this shot were $2.1x10^{23}$ cm^{-3} and $1.0x10^{23}cm^{-3}$ for the Heβ and Lyβ lines respectively. This was in reasonable agreement with the hydrocode simulations. However, at later times the density inferred from the line widths did not fall below around $5x10^{22}cm^{-3}$. This was not in agreement with the hydrocode which predicted that the density should fall of in a similar manner to the solid targets. The reason for this discrepancy is not clear as the irradiation conditions were similar and the crystal set-up identical to that for solid targets. The line ratios predicted are also in worse agreement than for solid aluminium, and indicate a colder plasma, than predicted by simulation. However, if the absorbed irradiance were much lower than predicted, we would not expect the K-shell emission observed to come from such high density plasma as indicated by the linewidths. Clearly more work on the hydrodynamic modelling of layered targets is needed.

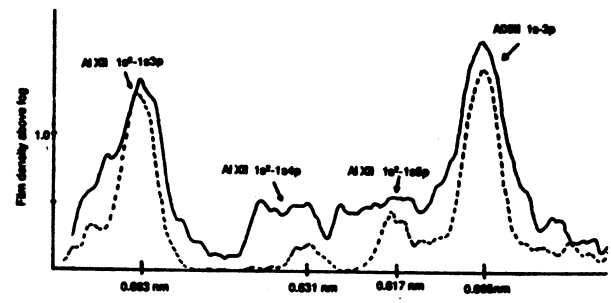

Figure 5. Film density line outs at (a) peak Lyβ emission and (b) 40ps later for a layered target at $6.4x10^{15}$ Wcm^{-2}

In conclusion, we have demonstrated the production of a rapidly heated plasma with a high brightness, pre-pulse free, Raman amplified KrF laser. The absence of a pre-formed plasma means that the plasma heating occurs at high density, with observed spectral features that differ markedly from previous observations with time integrated spectroscopy. In support of the measurement of high electron density from the Stark linewidths, we have clearly observed the time evolution of line series merging for the He-like aluminium lines. We consider that the fair agreement between the predicted and experimentally inferred electron density and temperature indicates that the plasma conditions are quite well modelled by the hydrocode, although more work is needed to understand our layered target data. In future, we intend to gain a fuller understanding of the ionisation dynamics, especially late in time, by developing time dependent detailed level accounting models.

The authors would like to thank the staff of the Central Laser Facility at the Rutherford Appleton Laboratory. We would also like to thank Dr J. Edwards for helpful discusions. This work was funded by a SERC research grant.

1. C.H. Nam, et. al Rev. Lett. **59**, 2427 (1987)
2. J.A. Cobble, et al. Phys. Rev. A. **39**, 454 (1989)
3. M.M. Murnane et al Phys. Rev. Lett. **62**, 155, (1989)
4. G.J. Tallents, M.H. Key, P. Norreys, D. Brown, J. Dunne and H. Baldis, Phys. Rev. A. **40**, 2857 (1989)
5. O. Willi, et. al Europhys. Lett., **10**, 141 (1989)
6. I.N. Ross, M.J. Shaw, C.J. Hooker, M.H. Key, E.C. Harvey, J.M.D. Lister J.E. Andrew, G.J. Hirst and P.A. Rodgers, Optics Communications, **78**, 263 , (1990) : E.C. Harvey, C.J. Hooker, J.R. Houliston, M.H. Key, A.K. Kidd, J.M.D. Lister, I.N. Ross, and M.J. Shaw, Rutherford-Appleton Laboratory Report RAL-91-025, 77
7. J. Stewart and K. Pyatt, Astrophysics J. **144**,1203(1966)
8. D.R. Inglis and E. Teller, Astrophysics J. ,**90**,439 (1939)
9. R.W. Lee, B.L. Whitten and R.E Stout II, J. Quant. Spectrosc. Radiat. Transfer, **32**, 91, (1984)
10. J.P. Christiansen, D.E.T.F. Ashby and K.V. Roberts, Computer Phys. Comm. **7**, 271, (1974)
11. G.J. Rickard, A.R. Bell, and E.M. Epperlein, Phys. Rev. Lett. **62**, 2687 (1989)
12. T.P Hughes *Proceedings of the XXth Scottish Summer School in Physics* eds. R.A. Cairns and J.J. Sanderson (SUSSP Publications Univ. Edinburgh 1979)
13. D.N. Giovanielli, Bull.Amer.Phys.Soc. SeriesII **9**, 1047
14. W.A. Lokke and W.H. Grasberger, Lawrence Livermore National Laboratory Report UCRL-52276 (1977): J. Edwards and S.J. Rose RAL report 91-025 (1991)
15 V.A. Barrow, Phd Thesis, University of London 1991
16. H.R. Griem *Plasma Spectroscopy*, McGraw-Hill, New York 1964